Langmuir

Article

pubs.acs.org/Langmuir

Bioactive Polymersomes Self-Assembled from Amphiphilic PPO-*Glyco*Polypeptides: Synthesis, Characterization, and Dual-Dye Encapsulation

Soumen Das,[†,#] Dharmendar Kumar Sharma,[§,#] Suman Chakrabarty,[‡] Arindam Chowdhury,*[,§] and Sayam Sen Gupta*[,†]

[†]Chemical Engineering Division and [‡]Physical and Materials Chemistry Division, CSIR-National Chemical Laboratory, Dr. Homi Bhabha Road, Pune 411008, India

[§]Department of Chemistry, Indian Institute of Technology Bombay, Powai, Mumbai 400076, India

Supporting Information

ABSTRACT: Glycopolypeptide-based polymersomes have promising applications as vehicles for targeted drug delivery because they are capable of encapsulating different pharmaceuticals of diverse polarity as well as interacting with specific cell surfaces due to their hollow structural morphology and bioactive surfaces. We have synthesized glycopolypeptide-*b*-poly(propylene oxide) by ROP of glyco-*N*-carboxyanhydride (NCA) using the hydrophobic amine-terminated poly(propylene oxide) (PPO) as the initiator. This block copolymer is composed of an FDA-approved PPO hydrophobic block in conjugation with hydrophilic glycopolypeptides which are expected to be biocompatible. We demonstrate the formation of glycopolypeptide-based polymersomes from the self-assembly of glycopolypeptide-*b*-poly(propylene oxide) in which the presence of an ordered helical glycopolypeptide segment is required for their self-assembly into spherical nanoscale (∼50 nm) polymersomes. The polymersomes were characterized in detail using a variety of techniques such as TEM, AFM, cryo-SEM, and light-scattering measurements. As a model for drugs, both hydrophobic (RBOE) and hydrophilic (calcein) dyes have been incorporated within the polymersomes from solution. To substantiate the simultaneous entrapment of the two dyes, spectrally resolved fluorescence microscopy was performed on the glycopeptide polymersomes cast on a glass substrate. We show that it is possible to visualize individual nanoscale polymersomes and effectively probe the dyes' colocalization and energy-transfer behaviors therein as well as investigate the variation in dual-dye encapsulation over a large number of single polymersomes. Finally, we show that the galactose moieties present on the surface can specifically recognize lectin RCA_{120}, which reveals that the polymersomes' surface is indeed biologically active.

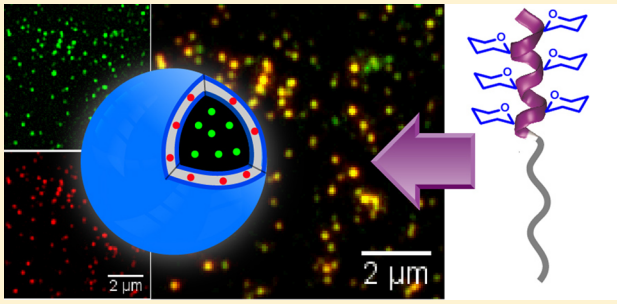

INTRODUCTION

The specific delivery of the therapeutic constituents of a drug to an organ, a tissue, or unhealthy cells using carriers is one of the major challenges in therapeutic research.[1] This requires the successful development of carrier systems that allow site-specific delivery of drugs such that they can act for long periods of time without affecting the normal cells.[2−4] Several nanocarrier-based delivery systems are being currently explored for such application.[5] Out of many potent nanocarriers, polymeric micelles or vesicles assembled from amphiphilic block copolymers have been a major research theme for drug delivery.[6] The micelles feature a hydrophobic core that can encapsulate hydrophobic drugs while the hydrophilic shell on its surface makes the entire assembly water-soluble. On the other hand, vesicles or polymersomes are hollow spheres that contain an aqueous solution in the core surrounded by a bilayered membrane. Because of this structural features, polymersomes can simultaneously encapsulate both hydrophilic and hydrophobic therapeutic molecule in their aqueous core and bilayer membrane, respectively.[7−9] Polymersomes have also been used as carriers for active drug delivery by using them to target to certain specific receptors on cell surfaces.[3,4,10−15] For example, targeting moieties such as RGD-containing peptides, folic acid, and carbohydrates have been displayed on the surface of polymersomes, and these have been used to target specific cancer cells.[16−23]

Polymersomes with carbohydrates on the surface represent a very interesting class of nanocarries because carbohydrates (found in glycoproteins) are involved in biomolecular recognition events[24−29] in vivo such as extracellular recognition, cell adhesion, cell growth regulation, cancer cell metastasis, and inflammation. Glycoprotein biomimetic polymersomes assembled from block copolymers containing polypeptide and oligosaccharide blocks have been synthesized,[26,30−32] and their

Received: October 8, 2014
Revised: February 21, 2015
Published: February 25, 2015

DOI: 10.1021/la503993e
Langmuir 2015, 31, 3402−3412

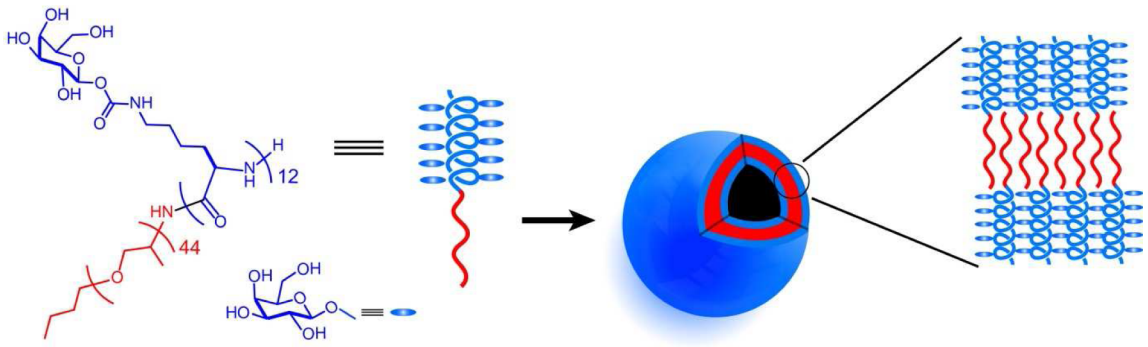

Figure 1. Schematic showing structures of amphiphilic block coglycopolypeptides and their assembly into polymersomes.

interaction with cells has been studied to understand their interactions with specific cell-surface receptors and their endocytosis mechanism. Recently, glycopolypeptide (GP; polypeptide backbone with pendant carbohydrate moieties)-based polymersomes have been synthesized by two different approaches. In 2012, Heise et al. reported the first glycopolypeptide-based polymersomes from poly(γ-benzyl-L-glutamate)-*block*-poly(propargylglycine) that was postsynthetically glycosylated using click chemistry.[33] In another approach, Deming et al. reported the formation of vesicles from amphiphilic diblock copolypeptides containing hydrophobic poly(L-leucine) and hydrophilic poly(α-D-galactopyranosyl-L-cysteine).[34] They show that only conformationally disordered glycopolypeptides segments favor the formation of quasi-spherical polymersomes with sizes of between ∼100 nm to several micrometers rather than rigid ordered α-helical glycopolypeptides.[34]

Simultaneous encapsulations of both hydrophilic and hydrophobic drugs into the core/shell regions of glycopeptide polymersomes are essential for their use as carriers for drug delivery. To understand the encapsulation properties of these polymersomes, hydrophobic and hydrophilic dyes are typically used as model drugs, and their encapsulation behavior is studied using fluorescence microscopy.[35]Although fluorescence imaging methods have been shown to be potentially useful, they have not been utilized effectively to study encapsulation behaviors within small (∼100 nm) polymersomes.[34,36] For instance, to illustrate that glycopeptide polymersomes can encapsulate two drug molecules, Deming et al. performed confocal microscopy using dyes of different polarity as well as emission colors.[34] Interestingly, these measurements could image only a subensemble of polymersomes which were relatively large (on the order of a few micrometers), where the presence of different dyes in the core (aqueous) and shell (hydrophobic) regions could be visualized. However, such experiments were unable to detect the much smaller (∼100 nm) polymersomes that have potential as realistic drug-delivery vehicles.[37] Thus, the ability of these small (∼100 nm) polymersomes to encapsulate two drugs of different polarity remains questionable. It is therefore imperative to be able to detect (image) individual nanoscale polymersome in a high-throughput manner and perform careful colocalization measurements to substantiate the presence of both hydrophobic and hydrophilic dyes within each polymersome. Being able to image single polymersomes would also allow one to understand the variability in encapsulation behaviors as well as open an avenue to test the ability of nanoscale polymersomes to infiltrate cellular environments.

We have recently reported the controlled generation of nanostructures (micelles and nanorods) in solution from amphiphilic linear−dendritic glycopolypeptide copolymers although the dendron part was not biocompatible.[38] We hypothesized that incorporating a nonpeptidic biocompatible hydrophobic backbone instead would widen the scope of the resultant polymeric assemblies and could help generate polymersomes which were not formed with glycopolypeptide−dendron conjugates. Poly(propylene oxide) (PPO), a well-known biocompatible FDA-approved polymer, was chosen as the hydrophobic block for conjugation with glycopolypeptides to obtain amphiphilic block copolymers. Examples of polypeptide assemblies incorporating PPO as the hydrophobic block have been reported in the literature.[39,40]

In this work, we report the synthesis and self-assembly of glycopolypeptide-*b*-poly(propylene oxide) in aqueous solution into polymersomes. This polypeptide was synthesized by the ring-opening polymerization (ROP) of glycol-*N*-carboxyanhydride (NCA) using hydrophobic amine-terminated PPO as the initiator. In contrast to prior reports on the formation of glycopolypeptide-based polymersomes,[33,34] we show that the presence of an ordered helical glycopolypeptide segment is required for their self-assembly into spherical nanoscale (∼50 nm) polymersomes, the morphology of which has been characterized both in solution as well as when cast on a substrate. In particular, Forster resonance energy transfer (FRET) measurements in solution using a hydrophilic donor (calcein) and a hydrophobic acceptor (RBOE) hint at both dyes being incorporated within the polymersomes. To corroborate the simultaneous encapsulation of the two dyes, energy-mapped fluorescence imaging and spectrally resolved microscopy were performed on polymersomes (cast on a glass substrate). We show that it is possible to visualize individual (spatially segregated) nanoscale polymersome with high contrast, which allowed us to effectively probe colocalization and energy-transfer behaviors of the hydrophobic and hydrophilic dyes within the same (individual) glycopeptide polymersome. Finally, our results show that the polymersomes' surface is indeed biologically active and the galactose moieties present on the surface of polymersomes can specifically recognize lectin RCA_{120}.

EXPERIMENTAL SECTION

Materials and Methods. Poly(propylene glycol) monobutyl ether(PPO−OH, M_n = 2500 g/mol) and rhodamine B octadecyl ester perchlorate (RBOE) were purchased from Sigma-Aldrich. calcein was purchase from Invitrogen, Life Technologies. Glyco-*N*-carboxyanhydride (glyco-NCA) was prepared by using our previously published methodology (Figure S1).[27] All other chemicals used were

DOI: 10.1021/la503993e
Langmuir 2015, 31, 3402−3412

Scheme 1. Synthesis of Hydrophobic Initiator PPO−NH_2

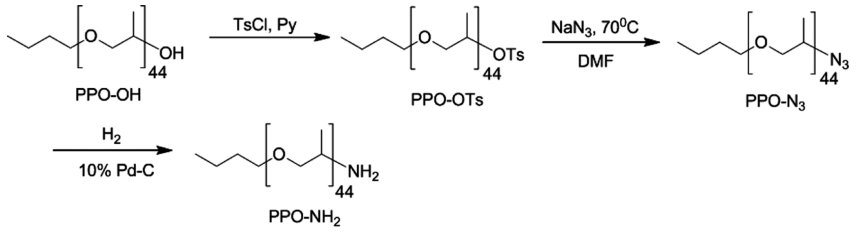

Scheme 2. Synthesis of amphiphilic blocks copolymers GP-PPO

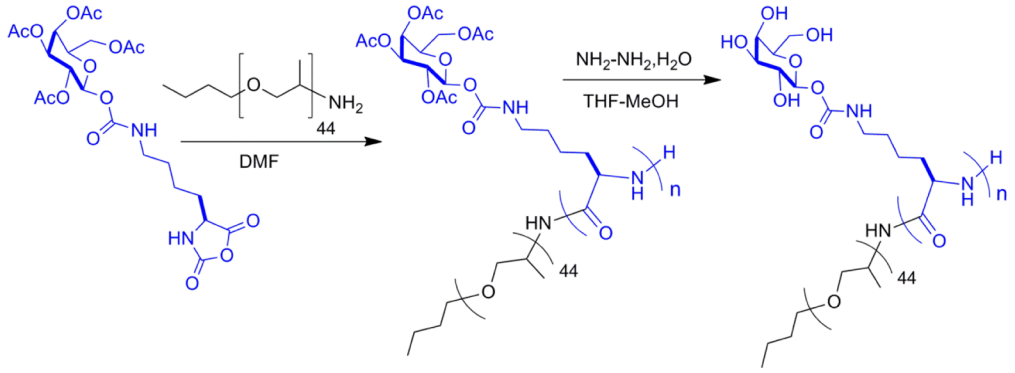

obtained from Merck, India. UV−vis spectra were recorded on a Cary-300 UV−vis spectrometer using a 1 cm quartz cuvette at 25 °C, and FT-IR spectra were recorded by using KBr pellets in a PerkinElmer FT-IR spectrum GX instrument. KBr pellets were prepared by mixing 97 mg of KBr with 3 mg of sample. ^{1}H NMR and ^{13}C NMR spectra were obtained with a Bruker spectrometer (200.13 and 400.13 MHz). Size exclusion chromatography of the polymer was performed with a Viskotek TDA 305-040 triple detector array GPC/SEC module. Separations were achieved with three columns (T6000M, general mixed ORG 300 × 7.8 mm^2) and one guard column (TGAURD, ORG guard col 10 × 4.6 mm^2) and 0.025 M LiBr in DMF as the eluent at 60 °C. GPC/LS samples were prepared at a concentration of 5 mg/mL. A constant flow rate of 1 mL/min was maintained, and the instrument was calibrated using PMMA standards. Polydispersity index (PDI) values were calculated using OmniSEC software. Transmission electron microscopy (TEM) measurements were performed at 100 kV on an FEI Technai T20 instrument. Atomic force microscopy (AFM) measurements and analysis were performed on a Nanoscope IV (Veeco). Cryo-field emission gun (FEG) scanning electron microscopy (SEM) was performed on a Jeol JSM-7600F instrument equipped with a cryo-prepartion system (pp3000T, Quorum Tech). The details of sample-preparation procedures for TEM, AFM, and cryo-SEM are provided in the Supporting Information. Steady-state fluorescence measurements were performed using a Horiba JobinYvon Fluorolog 3 spectrophotometer.

Synthesis of Amine-Terminated Poly(propylene glycol) Monobutyl Ether (PPO−NH_2). Poly(propylene glycol) monobutyl ether (PPO−OH) (10 g, 4 mmol) was dissolved in 50 mL of pyridine, and *p*-toluenesulfonyl chloride (7.6 g, 40 mmol) was added to the solution (Scheme 1). The reaction mixture was stirred for 24 h at room temperature and then poured into 50 mL of ice-cold 6 M HCl solutions. The product was extracted with methylene chloride, and the solvent was removed under vacuum. The oily PPO-OTs was purified by quickly passing through a silica gel column. The purified product was then dissolved in 20 mL of DMF, and sodium azide (10 equiv) was added to the solution. The reaction mixture was stirred at 70 °C for 24 h. The reaction mixture was filtered through Whatman filter paper to remove residual sodium azide and then poured into ice-cold 6 M HCl solutions. The precipitated product was extracted using methylene chloride, and the organic layer was washed with 3 × 200 mL of cold water and dried over sodium sulfate. The solvent was removed under vacuum, and the obtained product was dried overnight under evacuated conditions. The terminal azide group of PPO−N_3 was then reduced to an amine via hydrogenation in the presence of 10% Pd/C catalyst. Colorless PPO−NH_2 was dried under vacuum and transferred into the glovebox. The final yield was 97%.

Synthesis of Block Copolymers Using Ring-Opening Polymerization. To a solution of glyco-NCA (100 mg/mL) in dry DMF was added "proton sponge" 1,8-bis(dimethylamino)naphthalene (1.0 equiv to monomer, 1 M) as an additive and PPO−NH_2 (0.5 M solution in dry DMF) as the initiator inside the glovebox (Scheme 2). The progress of the polymerization was monitored by FT-IR spectroscopy by comparing with the intensity of the initial NCA's anhydride stretching at 1785 and 1858 cm^{-1} (Figure S2). The reaction was generally completed within 16 h. Then the solvent from the reaction mixture was removed under reduced pressure. The resulting residue was redissolved in dichloromethane, and then the polymer precipitated out by the addition of diethyl ether. The precipitated polymer was collected by centrifugation and dried to afford gummy solid glycopolypeptide AcGP-PPO in almost 90% yield.

Deprotection of the Acetyl Protecting Group of AcGP-PPO Copolymers. Hydrazine monohydrate (25 equiv) was added to solutions of acetyl-protected AcGP-PPO block copolypeptides in THF−MeOH (1:1), and the reactions were stirred for 7 to 8 h at room temperature (Scheme 2). Reactions were quenched by the addition of acetone, and then solvent was removed almost completely under reduced pressure. The solid residues were dissolved in deionized water and transferred to dialysis tubing (3.5 kDa molecular weight cutoff). The samples were dialyzed against deionized water for 3 days, with water changes once every 2 h for the first day and then three times per day. Dialyzed polymers were lyophilized to yield glycopolypeptides as white fluffy solids (90% yields).

Assembly of Deprotected GP-PPO Copolymers in Aqueous Solution. Block-*co*-polymer (5.0 mg) was dissolved in 500 μL of DMSO by sonication and then filtered through a 0.22 μm GVWP membrane. Then the solution was placed into a 10 mL RB under magnetic stirring. After 2 min, 4.5 mL of ultrapure water was added instantaneously (<2 s) and stirred for another 2 h. The mixture was dialyzed for 24 h against deionized water (12 kDa molecular weight cut off) to remove DMSO.

Dynamic and Static Light Scattering. The variable-angle dynamic (DLS) and static (SLS) light-scattering experiments were carried out using a 3D-DLS spectrometer from LS Instruments,

DOI: 10.1021/la503993e
Langmuir 2015, 31, 3402−3412

Switzerland. The instrument consists of a He Ne laser having a wavelength of 632.8 nm, a variable-angle detection system, a temperature-controlled index-matching vat (LS Instruments), and toluene used as reference. The copolymer solutions were maintained at a constant temperature of 25 °C during the experiments. Dynamic light scattering measurements were carried out from 30 to 120° in steps of 10° and then evaluated by fitting the measured normalized time autocorrelation function of the scattered light intensity. The fluctuations in scattering intensity were analyzed via the intensity autocorrelation function ($g^{(2)}(\tau)$), where τ is the relaxation time. Apparent diffusion coefficients D_{app} were obtained by plotting the relaxation frequency Γ ($\Gamma = 1/\tau$) versus q^2, where q is the wave vector defined as

$$q = \frac{4\pi n}{\lambda} \sin(\theta/2)$$

where λ is the wavelength of the incident laser beam (632.8 nm), θ is the scattering angle, and n is the refractive index of the solvent. The hydrodynamic radius (R_h) was then calculated from the Stokes–Einstein equation

$$D_{app} = \frac{k_B T}{6\pi\eta R_h}$$

where η is the viscosity of the solvent and k_B is Boltzmann's constant.

In SLS experiments, the scattering intensity $I_s(q)$ is measured as a function of scattering angle θ which has been varied from 30° to 120° in steps of 2°, providing a q range from 7×10^{-4} to 2.0×10^{-3} Å^{-1}. The radius of gyration R_g can be calculated from the logarithm plot of the Guinier equation

$$\ln I_s(q) = \ln I_i - \frac{q^2 R_g^{\ 2}}{3}$$

Circular Dichroism Measurements. Solutions of polymers were filtered through 0.22 μm syringe filters. Circular dichroism (CD) spectra (190–250 nm) of the GP-PPO block copolymer (0.25 to 1.0 mg/mL in acetonitrile or in deionized water) were recorded (Jasco CD spectropolarimeter, J-815) in a cuvette with a 1 mm path length. All of the spectra were recorded for an average of three scans, and the spectra were reported as a function of molar ellipticity $[\theta]$ versus wavelength. The molar ellipticity was calculated using the standard formula $[\theta] = (\theta \times 100 \times M_w)/(C \times l)$, where θ is the experimental ellipticity in mdeg, M_w is the average molecular weight, C is the concentration in mg/mL, and l is the path length in cm. The percent α helicity was calculated by using the expression % α-helicity = $(-[\theta]222$ nm + 3000)/39 000.

Dye Encapsulation into Polymersomes. GP-PPO copolymers are assembled into polymersomes in an aqueous medium so that they can encapsulate hydrophilic as well as hydrophobic dyes. The encapsulation of hydrophilic dye calcein into the polymersomes was done by the coassembly method. First, polymer (5.0 mg) was dissolved in 475 μL of DMSO by sonication, and to that 25 μL of calcein solution (2 mg/mL in DMSO) was added. Then the solution was placed into a 10 mL RB under magnetic stirring. After 2 min, 4.5 mL of ultrapure water was added instantaneously (<2 s) and stirred for another 2 h. The mixture was placed into a dialysis membrane (12KDa molecular weight cutoff) and then dialyzed against phosphate buffer (pH 8.0) containing 50 mM phosphate, 50 mM NaCl, 0.2 mM disodium salt of EDTA. Within 16 h, all the unencapsulated calcein came out of from inside the dialysis membrane. After the removal of free calcein, the mixture was dialyzed against deionized water for 24 h with the water being changed three times. Hydrophobic dye RBOE was encapsulated after the formation of the polymersomes. For example, 100 μL of RBOE solution (0.5 mg/mL in acetone) was added to 5 mL of polymersomes solution (1.0 mg/mL) under stirring. After 6 h, with the evaporation of the added acetone, all of the RBOE that was not incorporated into the polymersomes precipitated out. The mixture was then filtered through 0.22 μm filter paper to remove precipitated RBOE. To encapsulate both calcein and RBOE dye into the same polymersomes, first calcein was encapsulated into the polymersomes by the coassembly method, and then that aqueous solution was used for the encapsulation of the hydrophobic RBOE dye.

Spectrally Resolved Imaging of Polymersomes. *Sample Preparation.* Polymersomes solution in water (20 μL) containing calcein and/or RBOE was drop cast on cleaned glass coverslips, and the solvent was evaporated at room temperature in the dark. Different concentrations of polymersomes (0.01, 0.03, and 0.1 mg/mL) containing the dyes were used to optimize the density of polymersomes so that spatially well-separated individual emission spots were visible (Supporting Information). Both the colocalization and energy-transfer (spectral) measurements were performed at a polymersome concentration of 0.1 mg/mL containing ~30 nM calcein and ~300 nM RBOE. Control experiments were performed to optimize the concentrations of both calcein and RBOE such that their fluorescence could be detected at high signal to background with 488 and 532 nm excitation sources, respectively.

Wide-Field Fluorescence Microscopy and Data Analysis. A home-built total internal reflection fluorescence (TIRF) microscopy setup based on an inverted optical microscope (Nikon TE2000U) was used to perform fluorescence energy-mapped imaging and to collect spatially resolved emission spectra of individual polymersomes in a high-throughput manner. Details of the experimental setup and data analysis procedures are provided elsewhere.[41,42] A 488 nm Ar ion and a 532 nm DPSS laser were used to illuminate a 40 × 40 μm^2 area of the sample via a 1.49 NA 60× objective (Nikon, Apo TIRF). Identical excitation power (2 W/cm^2 as measured below the objective) for the two laser lines was used to illuminate both calcein and RBOE. The fluorescence emission from individual spots was collected using the same objective lens, passed through respective dichroic mirrors and notch filters as well as a broad band (500–700 nm) emission filter (Semrock), and eventually imaged through a cooled interline CCD camera (DVC 1412AM) at 100 ms exposure. To obtain qualitative information on the colocalization of two dyes, fluorescence imaging was performed on the same sample area using band-pass filters for calcein (490–530 nm, FF01-510/42-25, Semrock) and RBOE (545–635 nm, HQ 590/90M, Semrock). The individual images (16-bit) collected using the two energetic filters (assigned green and red colors) were quantitatively superimposed via pixel-by-pixel matching to generate a pseudocolor energy-mapped image, where the shade of each spot qualitatively represents the intensities measured in individual detection channels. All images were analyzed after background flattening (rolling ball radius of 50 pixels) due to slight modulations in the excitation field. Spatially resolved fluorescence spectroscopy of individual spots was performed using a combination of a narrow slit and a transmission grating (70 g/mm) placed in front of the CCD detector.[41,42] The emission profiles were calibrated for pixel to nanometer conversion using several laser lines and also corrected for the detector wavelength response. All spectrally resolved images (Supporting Information) via dual-wavelength excitation (488 and 532 nm) were collected at identical excitation powers (2W/cm^2) and exposure times (300 ms). To avoid misinterpretation of in energy-transfer due to photobleaching, emission spectra from each sample area were first collected for 532 nm followed by 488 nm excitation. Control measurements were performed on a single polymersome in the presence of the same amount of acceptor (RBOE) in the absence of the donor (calcein). All measurements were carried out at 25 °C, and data were analyzed using ImageJ (NIH) and Origin 7.5.

Recognition of the Galactose Residues of Polymersomes by Lectin. RCA_{120} interactions with vesicles were studied in 100 mM phosphate buffer solution (pH 7.2) containing 0.1 M NaCl, 0.1 mM $CaCl_2$, and 0.1 mM $MnCl_2$. RCA_{120} (1.0 and 0.5 mg/mL in this PBS buffer) was prepared and subsequently sterile filtered. Turbidity measurements were performed by adding 200 μL of the RCA_{120} solution to a dry quartz microcuvette (1 cm path length). A solution of the assembled polymersome solution in PBS buffer was then gradually added to the RCA_{120} solution. Upon addition, the solution was mixed vigorously for 10 s using a vortex mixer and then placed in the spectrometer to record the absorbance at 440 nm.

Molecular Dynamics Simulations. Extensive atomistic molecular dynamics (MD) simulations of the 12GP (all-L-amino acid) and *rac*-

DOI: 10.1021/la503993e
Langmuir 2015, 31, 3402–3412

Table 1. GP-PPO Block Copolymers Synthesized

	protected polymer					deprotected polymer		
polymer	M/I[a]	M_n (10^3g/mol)[b]	M_w/M_n[c]	DP[d]	% yield[e]	polymer	secondary structure[f]	hydrophilic wt %
12AcGP-PPO	12	8.9	1.10	14	96	12GP-PPO	helix	~62
rac-12AcGP-PPO	12	8.9	1.10	14	97	*rac*-12GP-PPO	nonhelical	~62
25AcGP-PPO	25	17.2	1.15	26	97	25GP-PPO	helix	~78

[a]Monomer to initiator ratio. [b]Number-average molecular weight calculated from GPC. [c]M_w/M_n was calculated from GPC. [d]DP was calculated from ^{1}H NMR. [e]Total isolated yield of the glycopolypeptides. [f]Secondary conformation in water determined from CD measurement.

12GP (equal D and L mixture with alternating D/L residues) were performed to understand the secondary structure content of the structural ensemble of the GPs in aqueous solution. All simulations and analyses were performed using the Gromacs (version 5.0.2) software suite.[43] The force field parameters of the GP residues were generated using the Antechamber utility of the AmberTools14 software suite.[44] RESP charges were calculated using multiconformational fitting of the electrostatic potential. All of the force field parameters were compatible with the AMBER99SB force field. All simulations were started from the linear conformation of both GPs. To speed up the sampling of the large conformational space of the polypeptide chains, extensive replica exchange molecular dynamics (REMD)[45] simulations were performed using 55 replicas in the temperature range of 300 to 400.56 K. All of the replicas were first equilibrated in the NPT ensemble for 50 ns. Replica exchanges were attempted every 4 ps. Production runs were continued for 450 ns, which amounts to a total run length of 24.75 μs over all replicas for each GP. The replica at 300 K was analyzed for the presence of various secondary structural elements for both GPs (all-L and equal D/L mixture) using DSSP.[46]

RESULTS AND DISCUSSION

Synthesis and Characterization of GP-PPO Block Copolymer. Amine-terminated PPO was synthesized by following the method of Savin et al. (Scheme 1).[40] PPO–OH was first tosylated, and the completion of tosylation was confirmed using ^{1}H NMR by integrating the peak at 2.39 ppm ($-SO_2-C_6H_4-CH_3$) with respect to PPO ($-CH-CH_3$) protons at 1.07–1.11 ppm (Supporting Information NMR spectra). In the next step, the tosyl group was quantitatively converted to the corresponding azide. The complete conversion was ascertained by monitoring the disappearance of resonance due to the tosyl group in ^{1}H NMR with the concomitant appearance of a peak at 2100 cm^{-1} in FT-IR due to the incorporation of the organo azide moiety. Finally, PPO–NH_2 was obtained by the reduction of PPO–N_3 and directly used as a macroinitiator for the ring-opening polymerization of NCA. The polymerization of α-D-galacto-L/LD-lysine NCA was carried out in the presence of 1.0 equiv of a proton sponge using PPO–NH_2 as the initiator (M/I = 12 and 25) in dry DMF (Scheme 2 and Table 1). The completion of the reaction was confirmed by the complete disappearance of the anhydride stretch of NCA at 1785 and 1858 cm^{-1} in the FT-IR spectra (Figure S2). The resulting block copolymer shows a monomodal, narrow-molecular-weight distribution in the GPC chromatogram (Figure S3). The molecular weight of the resulting polymer was also confirmed by ^{1}H NMR by integrating the PPO protons ($-CH-CH_3$) with respect to the acetyl protons of the GP segment (Supporting Information NMR spectra). The acetyl protecting groups of the pendant carbohydrate were completely removed by hydrazine hydrate. The complete removal of acetyl groups was confirmed by the absence of acetyl protons in the ^{1}H NMR spectra of GP-PPO in DMSO (Supporting Information NMR spectra).

The conformation of the GPs in solution was investigated by circular dichroism (CD). The GP segments in AcGP-PPO (Figure S4) and GP-PPO (Figure 2), all of which contain an enantiomerically pure poly-L-lysine backbone, were found to be α-helical in acetonitrile and water, respectively, with characteristic minima at 208 and 222 nm. In contrast, *rac*-AcGP-PPO and *rac*-GP-PPO polymers (polypeptide backbone of poly-DL-lysine) showed no helicity in the CD measurements (Figure 2). This was expected because a backbone containing a racemic amino acid is not expected to fold into an α-helix as has been shown by us before.[27]

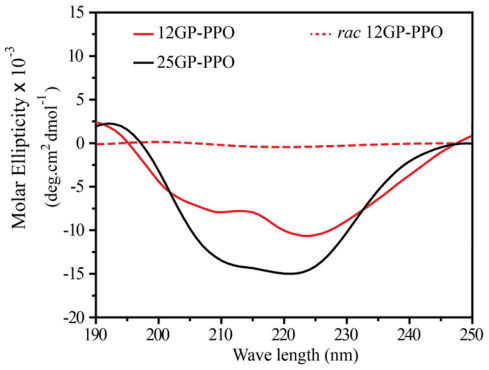

Figure 2. Circular dichroism spectra of the GP-PPO block copolymer in water at 25 °C.

Self-Assembly of GP-PPO Block Copolymer in an Aqueous Medium. Block copolymer consisting of two chemically dissimilar blocks undergo self-assembly in selective solvents, i.e., a good solvent for one block and a poor solvent for another block.[47] When water (poor solvent for the PPO segment at room temperature) was added to the GP-PPO polymer solution in DMSO (common solvent for both segments), the diffusion of DMSO into water forces the PPO segment to undergo microphase separation. During this process, the hydrophobic PPO chains tend to associate together in the polar environment, leading to the self-assembly of GP-PPO polymers. After the removal of DMSO by dialysis, a drop of the solution was deposited on a carbon-coated grid and analyzed by TEM using uranylaceate as a negative staining agent. We found that 12GP-PPO formed well-dispersed polymersomes with spherical structure (Figure 3a), and a characteristic dark rim on the outer surface (Figure 3a, inset) was indicative of their hollow morphology. Using TEM size distribution analyses (Figure S6a–c), it was observed that polymersomes cast on a surface under solvent-evaporated conditions have an average diameter of ~50 nm, with sizes ranging between ~30 and 70 nm (Figure S6c). Further evidence of the polymersomes' hollow nature was obtained from AFM measurements of the self-assembled structures on a silicon wafer (Figure 3b). AFM height analyses (Figure S5)

DOI: 10.1021/la503993e
Langmuir 2015, 31, 3402–3412

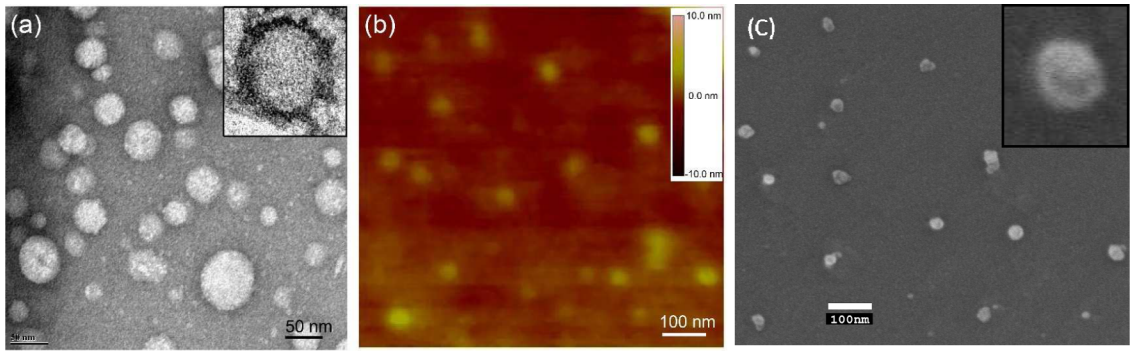

Figure 3. (a) TEM images of 12GP-PPO polymersomes in water with uranyl acetate as a negative stain and (b) AFM image of the polymersomes drop cast from aqueous solution on a silicon wafer. The inset of (a) shows the TEM blowup of a single polymersome. (c) Cryo-FEG-SEM image of 12GP-PPO polymersomes in water. The inset of (c) shows a cryo-SEM blowup of a single polymersome.

reveal the formation of circular discs with a thickness of ∼6−8 nm and a height/diameter ratio of ∼0.08, in good agreement with the hollow vesicular morphology.[48] In addition, cryo-FEG-SEM measurements were performed to obtain information on the morphology of the polymersomes in their native (solution) state, which not only show spherical structures (Figure 3c) but also suggest a hollow morphology. The size distribution of polymersomes obtained from cryo-SEM image analysis (Figure S7a,b) yielded a mean diameter of ∼44 nm with a range of 20−70 nm.

Light-scattering experiments (DLS and SLS) were then performed to obtain more information about size and morphology of the self-assembled structures in solution (Figure 4a,b). The hydrodynamic radius (R_h) was determined to be

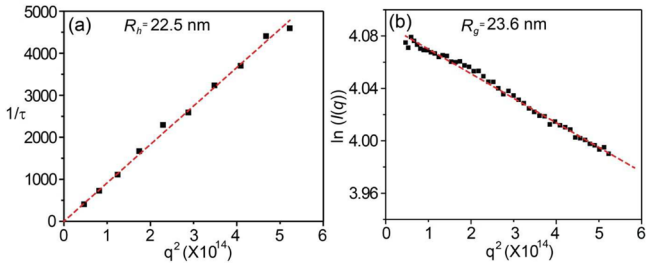

Figure 4. Multiangle light-scattering experiments on 12GP-PPO. (a) Plot of $1/\tau$ vs q^2 and R_h determination. (b) Guinier plot and R_g determination.

22.5 nm by multiangle DLS. In SLS experiments, the intensity of the scattered light measured at different angles is plotted against q^2, where q is the magnitude of the scattering vector. From the slope of the linear fitting, the radius of gyration (R_g) value was calculated to be 23.6 nm. The form factor (R_g/R_h) was found to be 1.06 for the 12GP-PPO polymer, which is close to the theoretical limit for polymersomes.[49] These values support the observations from electron microscopy and AFM measurements (Figure 3), and the diameters of polymersomes extracted from light-scattering measurements (45−47 nm) are in good agreement with the mean size obtained from cryo-SEM analysis (∼44 nm), substantiating the formation of nanoscale self-assembled hollow structures.

Generally, amphiphilic block copolymers with a hydrophilic to hydrophobic ratio larger than 1.0 usually form micelles, while those with a ratio of less than 0.5 tend to form polymersomes.[50] 12 GP-PPO, which has a hydrophilic to hydrophobic ratio of ∼1.6, is therefore expected to form micelles. However, all of our analytical data indicates the formation of polymersomes. We hypothesized that the conformationally rigid glycopolypeptide comprising of pure L-*glyco*-amino acid was critical to the self-assembly process leading to the formation of polymersomes. To test this hypothesis, *rac*-12GP-PPO polymer containing equal mixture of D- and L-*glyco*-amino acid was synthesized. The CD spectrum of this polymer shows the absence of helicity, and the glycopolypeptide chain exists in a more random conformation (Figure 2). We find that the *rac*-12GP-PPO polymer did not self-assemble into polymersomes in water and instead a sheetlike structure was observed (Figure S7d). This suggests a strong correlation between the secondary structure of the GP and nanoparticle structure formed upon self-assembly. A similar correlation between the helicity of GP and the structure of nanoparticles formed after self-assembly has been reported for GP−dendron conjugates in aqueous solution.[32] This is in stark contrast to two previous reports on glycopeptide-based polymersomes, where the conformationally disordered hydrophilic glycopeptide segments favor the formation of vesicles; in these amphiphiles, the formation of polymersomes was driven by the packing of a helical hydrophobic segment.[33,34] On the contrary, our results clearly demonstrate that the 12-mer glycopolypeptide, which exists only as a weak helix (∼28% helicity), has a strong correlation with the formation of polymersomes, which is indeed very intriguing.

To understand the role of the weakly helical glycopolypeptide in the self-assembly process, we first studied the structural ensemble of both pure and *rac*-glycopolypeptide by MD simulations. It was observed that 12GP exhibits a considerable helix−coil dynamic equilibrium, where the helical content is found to be divided between α-helices and 3−10 helices. The overall population distribution of various secondary structural elements for 12GP is found to be α-helix, 21%; 3−10 helixes, 28%; turn, 23%; and coil, 24% (Figure 5). As we would expect, *rac*-12GP does not demonstrate any appreciable helical content. It primarily exists in a disordered coil structure (50%) with a smaller population of turns (23%) and bends (25%) (Figure 5). These results are in reasonable agreement with the experimental CD spectra (Figure 3) as well. On the basis of above conformational analysis of the glycopolypeptides, the structure of amphiphiles 12GP-PPO and *rac*-12GP-PPO would be expected to be roughly helix−coil and coil−coil, respectively. Even though the helical peptide appears to be quite flexible and dynamic in solution, we think that the conformational equilibrium can shift further toward the helical structures

DOI: 10.1021/la503993e
Langmuir 2015, 31, 3402−3412

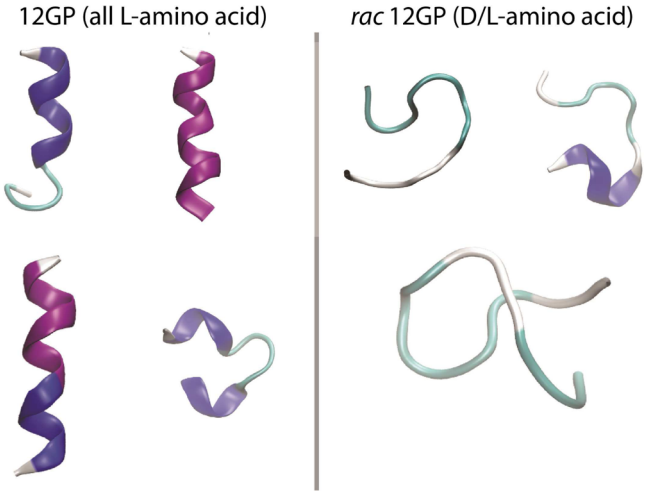

Figure 5. Representative snapshots from the extended structural ensemble (REMD) as observed from the replica at 300 K for both 12GP (left panel) and *rac*-12GP (right panel). Only the cartoon representation of the backbone is shown for clarity. The highlighted secondary structural elements are α-helix (purple), 3−10 helix (blue), turn (cyan), and coil (white).

once the self-assembly process is initiated by the hydrophobic association of the PPO segments. The helical conformation of 12GP (Figure S8) would certainly provide more efficient packing of the peptide segment on the surface of the polymersomes, and thus the population of the helical structures is likely to be enhanced in the polymersomes. In contrast, the inability to form helices would not allow the *rac*-12GP-PPO polymers to form a compact self-assembled structure due to a larger hydrodynamic radius with higher sphericity. Further work is in progress to study the stabilization of the helical conformation of the peptides induced by the self-assembly process.

Finally, upon increasing the hydrophilic/hydrophobic ratio of GP-PPO to 3.5, resultant polymer 25GP-PPO assembled into wormlike micelles (Figure S7e), suggesting that a longer hydrophilic GP chain in 25GP-PPO induced the assembly of this polymer into a morphology bearing higher curvature.

Dye-Encapsulation Studies. The hollow nature of the spherical particles was tested by encapsulating hydrophilic dye calcein. UV−vis spectra of dye-encapsulated 12GP-PPO polymersomes show a characteristic peak (λ_{max}) at 493 nm (Figure 6a). The encapsulation efficiency (EE) was determined using the expression EE = $(W_1/W_2) \times 100$, where, W_1 is the amount of calcein encapsulated and W_2 is the amount of calcein taken in the feed. The value of W_1 was estimated from the optical density (OD) at 493 nm (extinction coefficient for calcein in water is 76 000 M^{-1} cm^{-1}), from which the encapsulation efficiency of calcein was determined to be ∼6.3%. The hydrophobic payload encapsulation of the polymersomes was checked using nonpolar dye RBOE, the long octadecyl chain of which makes it suitable to be placed within the hydrophobic membrane of the vesicles. The encapsulation efficiency of RBOE (extinction coefficient in methanol is 112 000 $M^{-1}cm^{-1}$) was calculated to be ∼23% by following the same expression as used for calcein. The UV−vis spectra of RBOE-encapsulated polymersomes ($\lambda_{max} \approx 562$ nm) show a clear blue shift (Figure S9) as compared to water ($\lambda_{max} \approx 569$ nm), which indicates that RBOE resides in a relatively nonpolar microenvironment, consistent with the hydrophobic shell of the polymersomes. Furthermore, DLS measurements (Figure S10) suggest that the encapsulation of dyes leads to an increase in the size of the polymersomes. To corroborate this, fluorescence correlation spectroscopy (FCS) was performed on very dilute (∼1 nM) aqueous solutions of 12GP-PPO polymersomes in the presence of RBOE (Figure S11). The diffusivities for the polymersomes extracted from the single-component fit to the intensity autocorrelation function revealed an average hydrodynamic radius of ∼42 nm. In addition, the absence of a fast decay (up to few hundred μs) in the observed FCS autocorrelation function points out that an overwhelming majority of hydrophobic RBOEs are sequestered within the polymersomes.

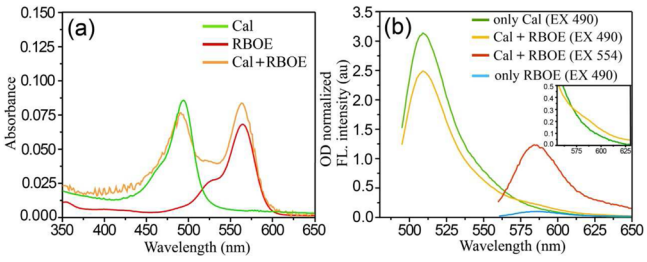

Figure 6. UV−vis absorption spectra of 12GP-PPO polymersomes in water after dye encapsulation (a) and the OD-normalized emission spectra of dye-labeled polymersomes (b) in solution excited at different wavelengths. The enhancement of RBOE emission in the presence of calcein is blown up in the inset.

The fluorescence emission spectra of calcein-encapsulated polymersomes in water show an emission maximum (λ_{max}^{em}) at 514 nm, whereas RBOE-encapsulated polymersomes show an emission maximum at 578 nm upon excitation at their respective absorption maxima (490 and 554 nm, respectively) (Figure 6b). Because of the considerable overlap of calcein emission with RBOE absorption (Figure S12), these two dyes can act as donor−acceptor FRET pairs. We hypothesize that if both dyes are encapsulated within the polymersomes then it is possible to observe some energy transfer between the donor and the acceptor, which should result in a decrease in calcein emission and a simultaneous enhancement in RBOE emission. Figure 6b shows the OD-corrected fluorescence emission spectra of calcein-encapsulated polymersomes in the absence and presence of RBOE. The emission spectra in the presence of both dyes display a noticeable shoulder at 578 nm due to RBOE in addition to characteristic calcein emission, which is indicative of some amount of energy transfer between the FRET pair. Furthermore, the OD-normalized emission spectra of RBOE-loaded polymersomes directly excited at 490 nm are found to have a much lower intensity at 578 nm as compared to that in the presence of calcein-loaded polymersomes. Although this difference in intensity is not significant, we do observe a reduction in the donor fluorescence at 514 nm in presence of the acceptor, which again suggests that some amount of energy transfer do occur between calcein and RBOE. However, the extent of energy transfer is clearly nominal, likely due to the relatively large size of the polymersomes (∼50 nm), where a considerable fraction of encapsulated calcein molecules remain within the encapsulated aqueous environment, quite far from the RBOE buried within the hydrophobic membrane of the polymersomes. Nonetheless, solution measurements do suggest the possibility of a small fraction of calcein molecules being in close proximity to RBOE yet cannot provide conclusive

DOI: 10.1021/la503993e
Langmuir 2015, 31, 3402−3412

evidence that both dyes are present within the same polymersome.

Spectrally Resolved Imaging of Individual Polymersome. To substantiate the encapsulation of both hydrophilic and hydrophobic dyes within the same polymersome, wide-field fluorescence microscopy was performed using 488 and 532 nm laser excitation on dye-loaded polymersomes drop-cast on a glass substrate. First, fluorescence imaging was performed for different concentrations of polymersomes in the presence of each dye individually, following which they were imaged in the presence of optimal proportions of both dyes. Figure S13 shows the presence of several bright, highly localized emission spots, the density of which increases with polymersome concentration (without a significant change in their intensity). This demonstrates that individual, spatially segregated polymersomes are being detected using either of the two dyes. Figure 7a shows the fluorescence intensity image of a characteristic area of the sample, where several tens of individual polymersomes can be readily visualized along with a few agglomerates. We find that a vast majority (70−80%) of these emission spots are diffraction-limited as expected for small polymersomes (≤200 nm) whereas the remaining ones with dimensions between 200 and 500 nm are relatively brighter because of the larger number of dyes likely to be accommodated therein (Figure S14). It should be noted that the relatively weak background signal due to nonspecifically bound dyes on the glass surface photobleaches at a much faster rate under continuous illumination as compared to those from localized emission spots, which provides additional evidence that the dyes are encapsulated within polymersomes.

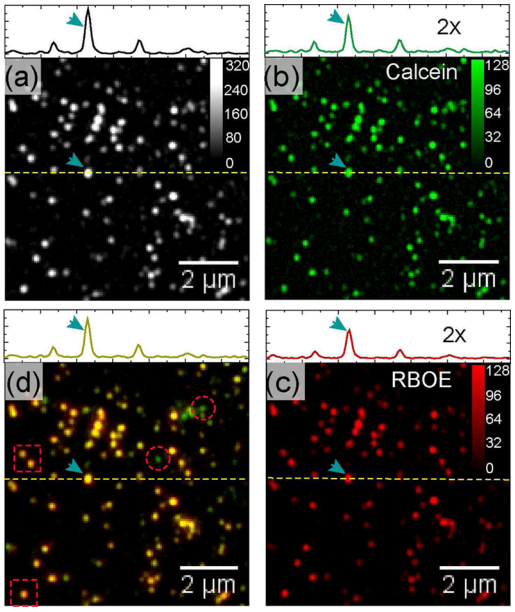

Figure 7. Energy-mapped fluorescence microscopy images for a characteristic area depicting individual polymersome as obtained through (a) 500−700 nm filter for the collective emission of calcein and RBOE, excited at 488 nm. (b) 490−530 nm filter for calcein emission (colored green) via 488 nm excitation, and (c) 545−635 nm filter for RBOE emission (colored red) via 532 nm excitation. The images were collected at same excitation power and exposure time. Superimposed pseudocolor intensity image (d) generated by the quantitative overlap of (b) and (c) to detect the colocalization of calcein and RBOE. Intensity line profiles (dashed lines) are shown on the top of each image for a comparison of quantitative intensities.

The colocalization of both dyes within individual polymersomes was probed using energy-mapped fluorescence imaging; the same sample area was excited with a 488 nm (for calcein) and a 532 nm (for RBOE) laser, following which the emission was collected via two energetically separated band-pass filters (490−530 nm and 545−635 nm) to selectively detect calcein and RBOE. Figures 7b and 7c show the intensity images of the same lateral area in detection of the emission from calcein (green, false color) and RBOE (red, false color), respectively. It is clear that an overwhelming majority of the emission spots show that both dyes are colocalized within individual polymersome (also seen from intensity line profiles in Figure 7). Furthermore, the intensity images from the two detection channels were quantitatively overlaid to generate a pseudocolor energy-mapped image (Figure 7d), where the hue of each spot qualitatively represents the relative abundance of two dyes within an individual polymersome. For instance, there are quite a few spots which either have more calcein (dotted circles, green tinge) or more RBOE (dotted squares, orange tinge) as compared to the predominant yellow color (similar intensities from both calcein and RBOE), signifying the variation in the relative proportion of two dyes among different polymersomes in the ensemble.

Interestingly, we noticed that when excited with a 488 nm laser (to visualize calcein), a large population of the polymersomes show significant emission in the lower energy-detection channel (for RBOE). This prompted us to explore energy transfer between the FRET pair within the polymersomes embedded on a glass substrate. To corroborate this possibility, spatially resolved fluorescence spectroscopy was performed on individual polymersomes in the presence of both the donor and acceptor dyes. First, the presence of acceptor (RBOE) was detected in each polymersome using 532 nm laser illumination followed by 488 nm excitation of the donor (calcein), and each time the emission spectral profile was collected for several polymersomes simultaneously as a spectrally resolved fluorescence image[41,42] (Figure S15a,b). Nine such characteristic single-polymersome fluorescence spectra under dual-wavelength excitation are shown in Figure 8a,b, along with the intensity image (Figure 8, inset) to identify each polymersome (spots marked 1−9) from which spectra were recorded. Here, we note that the extinction coefficient for RBOE at 532 nm is ∼6 times greater compared to that at 488 nm, and calcein can hardly absorb light at 532 nm (Figures S12 and S15). As a consequence, when excited at 532 nm, the emission spectra for individual polymersome displayed only characteristic RBOE emission (Figure 8a). Upon illumination of the (same) polymersome with a 488 nm laser at an identical laser power (Figure 8b), we find two distinct spectral envelopes due to calcein ($\lambda^{em}_{max} \approx 515$ nm) as well RBOE ($\lambda^{em}_{max} \approx 580$ nm). Interestingly, for 488 nm excitation, a majority of individual polymersome exhibit RBOE emission intensity (dashed box) only slightly less (2- to 3-fold) than that for selective excitation at 532 nm. This is in stark contrast to the more than 6-fold reduction in the emission intensity observed for RBOE (at λ_{ex} = 488 nm) within individual polymersomes in the absence of calcein (Figure 8a,b, dotted lines and Figure S16), which implies a considerable enhancement of the acceptor emission in the presence of the donor.

This emission intensity enhancement of RBOE no doubt points to significant energy transfer between the two dyes

DOI: 10.1021/la503993e
Langmuir 2015, 31, 3402−3412

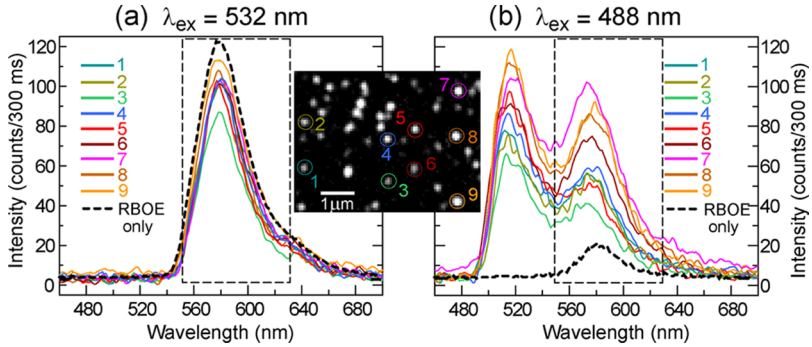

Figure 8. Spatially resolved fluorescence spectra of individual polymersomes using dual-wavelength excitation in the absence of emission filters. The intensity image (inset) identifies each emission spot from which spectra were collected (marked using color-coded circles and numbers). Representative emission profiles acquired from single polymersomes with (a) 532 nm and (b) 488 nm excitation. Spectra from each polymersome are color coded for a comparison of the RBOE emission window (dashed box) when excited at 532 and 488 nm. Thick dotted lines in (a) and (b) represent the emission spectra for an RBOE-labeled polymersome in the absence of calcein.

encapsulated within a single polymersome. Although it is not possible to quantify the extent of energy transfer (or the efficiency) due to a lack of information on the absolute number of (or proportions of) donor and acceptor dyes within each polymersome, we do find that there is a large variation in the extent of intensity enhancement (for RBOE) among different polymersomes in the subensemble (Figure S15c,d). It is rather difficult to comment whether this nonuniformity is a consequence of heterogeneity in size/shape of the polymersomes being probed, or is due variation in relative proportion of encapsulated dyes, or both. We note, however, that AFM measurements (Figure S5) reveal the formation of disc-shaped structures with height ranging between 5 and 10 nm when cast out of solution, which implies the collapse of the polymersome structure on a glass substrate. This can indeed result in a larger proportion of the donor and acceptor dyes being in close proximity (within the Förster radius) to allow for efficient energy transfer to take place. Nonetheless, these results, in conjunction with colocalization measurements, unambiguously demonstrate the capability of these PPO-glycopeptide polymersomes to encapsulate both hydrophobic and hydrophilic drugs concurrently.

Recognition of the Galactose Residues in Polymersomes by Lectin. The recognition and binding abilities of the galactose-containing polymersomes with RCA_{120} were estimated by turbidimetric assay (Figure 9). Protein RCA_{120} is known to bind specifically to galactosyl residues. In polymersomes, multiple copies of the galactosylated glycopolypeptides are displayed on the outer surface, and they are expected to interact with the carbohydrate binding site of the RCA_{120}. As can be observed for the addition of polymersome solution to the RCA_{120} solution, the turbidity first increases with increasing concentration and finally reaches a plateau. At this point, the turbidity does not increase with increasing concentration of polymersomes and can be considered to be an optimum value for the binding to RCA_{120}. As the concentration of RCA_{120} increased, the concentration of polymersomes also increased to completely precipitate out the RCA_{120}, as evidenced from Figure 9. This implies that the galactose moieties present at the surface of the polymersomes are available to interact with cell–surface receptors.

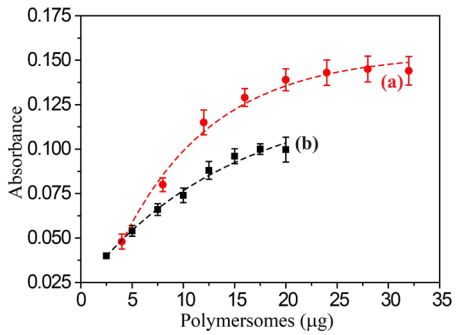

Figure 9. Turbidity assay of 12GP-PPO polymersomes at two different RCA_{120} concentrations of (a) 1.0 and (b) 0.5 mg/mL.

CONCLUSIONS

We have synthesized glycopolypeptide-*b*-poly(propylene oxide) by ROP of glyco-*N*-carboxyanhydride using hydrophobic amine-terminated PPO as the initiator with good control over molecular weight. This block copolymer is composed of a FDA-approved PPO hydrophobic block in conjugation with hydrophilic glycopolypeptides which are expected to be biocompatible. We demonstrate the formation of glycopolypeptide-based polymersomes from the self-assembly of glycopolypeptide-*b*-poly(propylene oxide) having 62% hydrophilicity by weight. We show that the packing of an ordered helical glycopolypeptide segment is essential for their self-assembly into spherical nanoscale polymersomes. This is in contrast to a recent report which suggests that random glycopolypeptide segments are required for polymersome formation. Specific recognition of lectin by the galactose moieties present on the polymersomes' surface reveals that these nanoscale vesicles are indeed biologically active. To evaluate their ability to encapsulate two drugs of different polarities, spectrally resolved microscopy was performed on polymersomes in the presence of a hydrophobic and a hydrophilic fluorescent dye. We show that it is possible to visualize individual, spatially segregated nanoscale (<100 nm) polymersomes with high contrast and in a high-throughput manner. This allowed us to effectively probe the colocalization and energy transfer of the dyes within the PPO-glycopeptide polymersomes and investigate the variation in the extent of dual-dye encapsulation. This demonstrated method could potentially be useful to understand the interaction of these dye-loaded polymersomes with cell surface receptors leading to endocytosis. Such studies are currently being performed in our laboratory.

DOI: 10.1021/la503993e
Langmuir 2015, 31, 3402–3412

■ ASSOCIATED CONTENT

Supporting Information

Experimental details of the synthesis, sample preparation, characterization, and NMR/optical spectroscopic data are provided, along with MD simulation snapshots and statistical data on single-particle fluorescence microscopy/spectroscopy. This material is available free of charge via the Internet at http://pubs.acs.org.

■ AUTHOR INFORMATION

Corresponding Authors

*E-mail: arindam@chem.iitb.ac.in.
*E-mail: ss.sengupta@ncl.res.in.

Author Contributions

#S.D. and D.K.S. made equal contributions to this work.

Notes

The authors declare no competing financial interest.

■ ACKNOWLEDGMENTS

S.D and D.K.S thank CSIR, New Delhi for fellowships. S.S.G thanks CSIR 12th FYP project CSC0302 for funding. We acknowledge Soumyajyoti Chatterjee for light-scattering measurements, Saibal Bhaumik for fluorescence measurements, and Dr. P. Rajmohanan for NMR support. A.C acknowledges IRCC IIT Bombay for initial funding, the AFM central facility (physics department), and the cryo-FEG-SEM central facility (chemical engineering department) of IIT Bombay and the department of chemistry for the use of central facility equipment. A.C thanks Naresh Patwari and Sudipta Maiti for usage of FCS setup funded by the Department of Information Technology (Govt. of India) grant no.12(4)/2007-PDD.

■ REFERENCES

(1) Farokhzad, O. C.; Langer, R. Impact of Nanotechnology on Drug. *ACS Nano* **2009**, *3*, 16−20.
(2) Mura, S.; Nicolas, J.; Couvreur, P. Stimuli-Responsive Nanocarriers for Drug Delivery. *Nat. Mater.* **2013**, *12*, 991−1003.
(3) Allen, T. M. Ligand-Targeted Therapeutics in Anticancer Therapy. *Nat. Rev. Cancer* **2002**, *2*, 750−763.
(4) Blanazs, A.; Armes, S. P.; Ryan, A. J. Self-Assembled Block Copolymer Aggregates: From Micelles to Vesicles and Their Biological Applications. *Macromol. Rapid Commun.* **2009**, *30*, 267−277.
(5) Ge, Z.; Liu, S. Functional Block Copolymer Assemblies Responsive to Tumor and Intracellular Microenvironments for Site-Specific Drug Delivery and Enhanced Imaging Performance. *Chem. Soc. Rev.* **2013**, *42*, 7289−7325.
(6) Robertson, J. D.; Patikarnmonthon, N.; Joseph, A. S.; Battaglia, G. Block Copolymer Micelles and Vesicles for Drug Delivery. *Engineering Polymer Systems for Improved Drug Delivery*; John Wiley & Sons, 2013; pp 163−188.
(7) Discher, D. E.; Eisenberg, A. Polymer Vesicles. *Science* **2002**, *297*, 967−973.
(8) Discher, D. E.; Ahmed, F. Polymersomes. *Annu. Rev. Biomed. Eng.* **2006**, *8*, 323−341.
(9) Marguet, M.; Edembe, L.; Lecommandoux, S. Polymersomes in Polymersomes: Multiple Loading and Permeability Control. *Angew. Chem., Int. Ed.* **2012**, *51*, 1173−1176.
(10) Discher, D. E.; Ortiz, V.; Srinivas, G.; Klein, M. L.; Kim, Y.; Christian, D.; Cai, S.; Photos, P.; Ahmed, F. Emerging Applications of Polymersomes in Delivery: From Molecular Dynamics to Shrinkage of Tumors. *Prog. Polym. Sci.* **2007**, *32*, 838−857.
(11) Onaca, O.; Enea, R.; Hughes, D. W.; Meier, W. Stimuli-Responsive Polymersomes as Nanocarriers for Drug and Gene Delivery. *Macromol. Biosci.* **2009**, *9*, 129−139.
(12) Liu, G.; Zhou, L.; Guan, Y.; Su, Y.; Dong, C. Multi-Responsive Polypeptidosome: Characterization, Morphology Transformation, and Triggered Drug Delivery. *Macromol. Rapid Commun.* **2014**, *35*, 1673−1678.
(13) Wei, R.; Cheng, L.; Zheng, M.; Cheng, R.; Meng, F.; Deng, C.; Zhong, Z. Reduction-Responsive Disassemblable Core-Cross-Linked Micelles Based on Poly(ethylene glycol)-b-poly(N-2-hydroxypropyl methacrylamide)-Lipoic Acid Conjugates for Triggered Intracellular Anticancer Drug Release. *Biomacromolecules* **2012**, *13*, 2429−2438.
(14) Wang, R.; Chen, W.; Meng, F.; Cheng, R.; Deng, C.; Feijen, J.; Zhong, Z. Unprecedented Access to Functional Biodegradable Polymers and Coatings. *Macromolecules* **2011**, *44*, 6009−6016.
(15) Deng, C.; Wu, J.; Cheng, R.; Meng, F.; Klok, H. A.; Zhong, Z. Functional Polypeptide and Hybrid Materials: Precision Synthesis via α-amino Acid N-carboxyanhydride Polymerization and Emerging Biomedical Applications. *Prog. Polym. Sci.* **2014**, *39*, 330−364.
(16) Liu, G.; Zhou, L.; Su, Y.; Dong, C. An NIR-responsive and Sugar-targeted Polypeptide Composite Nanomedicine for Intracellular Cancer Therapy. *Chem. Commun.* **2014**, *50*, 12538−12541.
(17) Zhong, Y.; Meng, F.; Deng, C.; Zhong, Z. Ligand-Directed Active Tumour-Targeting Polymeric Nanoparticles for Cancer Chemotherapy. *Biomacromolecules* **2014**, *15*, 1955−1969.
(18) Upadhyay, K. K.; Le Meins, J.-F.; Misra, a; Voisin, P.; Bouchaud, V.; Ibarboure, E.; Schatz, C.; Lecommandoux, S. Biomimetic Doxorubicin Loaded Polymersomes from Hyaluronan-Block-Poly(γ-Benzyl Glutamate) Copolymers. *Biomacromolecules* **2009**, *10*, 2802−2808.
(19) Chen, G.; Amajjahe, S.; Stenzel, M. H. Synthesis of Thiol-Linked Neoglycopolymers and Thermo-Responsive Glycomicelles as Potential Drug Carrier. *Chem. Commun.* **2009**, 1198−1200.
(20) Cho, C. S.; Seo, S. J.; Park, I. K.; Kim, S. H.; Kim, T. H.; Hoshiba, T.; Harada, I.; Akaike, T. Galactose-Carrying Polymers as Extracellular Matrices for Liver Tissue Engineering. *Biomaterials* **2006**, *27*, 576−585.
(21) Holowka, E. P.; Sun, V. Z.; Kamei, D. T.; Deming, T. J. Polyarginine Segments in Block Copolypeptides Drive Both Vesicular Assembly and Intracellular Delivery. *Nat. Mater.* **2007**, *6*, 52−57.
(22) Otsuka, H.; Nagasaki, Y.; Kataoka, K. PEGylated Nanoparticles for Biological and Pharmaceutical Applications. *Adv. Drug Delivery Rev.* **2003**, *55*, 403−419.
(23) Wu, D. Q.; Lu, B.; Chang, C.; Chen, C. S.; Wang, T.; Zhang, Y. Y.; Cheng, S. X.; Jiang, X. J.; Zhang, X. Z.; Zhuo, R. X. Galactosylated Fluorescent Labeled Micelles as a Liver Targeting Drug Carrier. *Biomaterials* **2009**, *30*, 1363−1371.
(24) Bertozzi, C. R. Chemical Glycobiology. *Science* **2001**, *291*, 2357−2364.
(25) Das, S.; Pati, D.; Tiwari, N.; Nisal, A.; Gupta, S. S. Synthesis of Silk Fibroin-Glycopolypeptide Conjugates and Their Recognition with Lectin. *Biomacromolecules* **2012**, *13*, 3695−3702.
(26) Bonduelle, C.; Lecommandoux, S. Synthetic Glycopolypeptides as Biomimetic Analogues of Natural Glycoproteins. *Biomacromolecules* **2013**, *14*, 2973−2983.
(27) Pati, D.; Shaikh, A. Y.; Das, S.; Nareddy, P. K.; Swamy, M. J.; Hotha, S.; Gupta, S. S. Controlled Synthesis of O-Glycopolypeptide Polymers and Their Molecular Recognition by Lectins. *Biomacromolecules* **2012**, *13*, 1287−1295.
(28) Manning, D. D.; Hu, X.; Beck, P.; Kiessling, L. L. Synthesis of Sulfated Neoglycopolymers: Selective P-Selectin Inhibitors. *J. Am. Chem. Soc.* **1997**, *119*, 3161−3162.
(29) Mammen, M.; Choi, S.; Whitesides, G. M. Polyvalent Interactions in Biological Systems: Implications for Design and Use of Multivalent Ligands and Inhibitors. *Angew. Chem., Int. Ed.* **1998**, *37*, 2754−2794.
(30) Schatz, C.; Louguet, S.; Le Meins, J.-F.; Lecommandoux, S. Polysaccharide-Block-Polypeptide Copolymer Vesicles: Towards Synthetic Viral Capsids. *Angew. Chem., Int. Ed.* **2009**, *48*, 2572−2575.
(31) Ladmiral, V.; Semsarilar, M.; Canton, I.; Armes, S. P. Polymerization-Induced Self-Assembly of Galactose-Functionalized

DOI: 10.1021/la503993e
Langmuir 2015, 31, 3402−3412

Biocompatible Diblock Copolymers for Intracellular Delivery. *J. Am. Chem. Soc.* **2013**, *135*, 13574−13581.
(32) Bonduelle, C.; Huang, J.; Ibarboure, E.; Heise, A.; Lecommandoux, S. Synthesis and Self-Assembly of "Tree-like" Amphiphilic Glycopolypeptides. *Chem. Commun.* **2012**, *48*, 8353−8355.
(33) Huang, J.; Bonduelle, C.; Thévenot, J.; Lecommandoux, S.; Heise, A. Biologically Active Polymersomes from Amphiphilic Glycopeptides. *J. Am. Chem. Soc.* **2012**, *134*, 119−122.
(34) Kramer, J. R.; Rodriguez, A. R.; Choe, U.-J.; Kamei, D. T.; Deming, T. J. Glycopolypeptide Conformations in Bioactive Block Copolymer Assemblies Influence Their Nanoscale Morphology. *Soft Matter* **2013**, *9*, 3389.
(35) Amstad, E.; Kim, S. H.; Weitz, D. A. Photo- and Thermoresponsive Polymersomes for Triggered Release. *Angew. Chem.* **2012**, *124*, 12667−12671.
(36) Das, A. K.; Mondal, T.; Sasmal, D. K.; Bhattacharyya, K. Femtosecond Study of Ultrafast Fluorescence Resonance Energy Transfer in a Catanionic Vesicle. *J. Chem. Phys.* **2011**, *135*, 074507.
(37) Win, K. Y.; Feng, S.S. Effects of Particle Size and Surface Coating on Cellular Uptake of Polymeric Nanoparticles for Oral Delivery of Anticancer Drugs. *Biomaterials* **2005**, *26*, 2713−22.
(38) Pati, D.; Kalva, N.; Das, S.; Kumaraswamy, G.; Sen Gupta, S.; Ambade, A. V. Multiple Topologies from Glycopolypeptide-Dendron Conjugate Self-Assembly: Nanorods, Micelles, and Organogels. *J. Am. Chem. Soc.* **2012**, *134*, 7796−7802.
(39) Naik, S. S.; Ray, J. G.; Savin, D. Temperature- and pH-Responsive Self-Assembly of Poly(propylene Oxide)-B-Poly(lysine) Block Copolymers in Aqueous Solution. *Langmuir* **2011**, *27*, 7231−7240.
(40) Naik, S. S.; Savin, D. Poly(Z-Lysine)-Based Organogels: Effect of Interfacial Frustration on Gel Strength. *Macromolecules* **2009**, *42*, 7114−7121.
(41) Layek, A.; De, S.; Thorat, R.; Chowdhury, A. Spectrally Resolved Photoluminescence Imaging of ZnO Nanocrystals. *J. Phys. Chem. Lett.* **2011**, *2*, 1241−1247.
(42) De, S.; Layek, A.; Raja, A.; Kadir, A.; Gokhale, M. R.; Bhattacharya, A.; Dhar, S.; Chowdhury, A. Two Distinct Origins of Highly Localized Luminescent Centers within InGaN/GaN Quantum-Well Light-Emitting Diodes. *Adv. Funct. Mater.* **2011**, *21*, 3828−3835.
(43) Van Der Spoel, D.; Lindahl, E.; Hess, B.; Groenhof, G.; Mark, A. E.; Berendsen, H. J. GROMACS: Fast, Flexible, and Free. *J. Comput. Chem.* **2005**, *26*, 1701−1718.
(44) Case, D. A.; Babin, V.; Berryman, J. T.; Betz, R. M.; Cai, Q.; Cerutti, D. S.; Cheatham, T. E., III; Darden, T. A.; Duke, R. E.; Gohlke, H.; Goetz, A. W.; Gusarov, S.; Homeyer, N.; Janowski, P., Kaus, J.; Kolossváry, I.; Kovalenko, A.; Lee, T. S.; LeGrand, S.; Luchko, T.; Luo, R.; Madej, B.; Merz, K. M.; Paesani, F.; Roe, D. R.; Roitberg, A.; Sagui, C.; Salomon-Ferrer, R.; Seabra, G.; Simmerling, C. L.; Smith, W.; Swails, J.; Walker, R. C.; Wang, J.; Wolf, R.M.; Wu, X.; Kollman, P. A. *AMBER 14*; University of California: San Francisco, CA, 2014.
(45) Sugita, Y.; Okamoto, Y. Replica-exchange Molecular Dynamics Method for Protein Folding. *Chem. Phys. Lett.* **1999**, *314*, 141−151.
(46) Joosten, R. P.; te Beek, T. A. H.; Krieger, E.; Hekkelman, M. L.; Hooft, R. W. W.; Schneider, R.; Sander, C.; Vriend, G. *Nucleic Acids Res.* **2011**, *39*, D411−D419.
(47) Mai, Y.; Eisenberg, A. Self-Assembly of Block Copolymers. *Chem. Soc. Rev.* **2012**, *41*, 5969−5985.
(48) Kazakov, S.; Kaholek, M.; Kudasheva, D.; Teraoka, I.; Cowman, M. K.; Levon, K. Poly (N-Isopropylacrylamide-Co-1-Vinylimidazole) Hydrogel Nanoparticles Prepared and Hydrophobically Modified in Liposome Reactors: Atomic Force Microscopy and Dynamic Light Scattering Study. *Langmuir* **2003**, 8086−8093.
(49) Houga, C.; Giermanska, J.; Lecommandoux, S.; Borsali, R.; Taton, D.; Gnanou, Y.; Le Meins, J. F. Micelles and Polymersomes Obtained by Self-Assembly of Dextran and Polystyrene Based Block Copolymers. *Biomacromolecules* **2009**, *10*, 32−40.
(50) Antonietti, M.; Förster, S. Vesicles and Liposomes: A Self-Assembly Principle Beyond Lipids. *Adv. Mater.* **2003**, *15*, 1323−1333.

DOI: 10.1021/la503993e
Langmuir 2015, 31, 3402−3412